EXPERIMENTAL STUDY ON DAMAGE DETECTION OF BASE-ISOLATED STRUCTURE USING AN ADAPTIVE EXTENDED KALMAN FILTER

Qiang Yin

School of Mechanical Engineering, Nanjing University of Science and Technology, Nanjing, China

e-mail: yinqiang@njust.edu.cn

Li Zhou, Tengfei Mu

State Key Laboratory of Mechanics and Control of Mechanical Structures,

Nanjing University of Aeronautics and Astronautics, Nanjing, China

Jann N. Yang

University of California, Department of Civil and Environmental Engineering, Irvine, USA

In this paper, experimental studies are performed and presented to verify the capability of the adaptive extended Kalman filter (AEKF) approach for identifying and tracking damages in nonlinear structures. A base-isolated building model consisting of a scaled building model mounted on a rubber-bearing isolation system has been tested experimentally in the laboratory. The non-linear behavior of the base isolators is represented by the Bouc-Wen model. To simulate the structural damages during the test, an innovative device, referred to as the stiffness element device (SED), is proposed to reduce the stiffness of the upper storey of the structure. Various damage scenarios have been simulated and tested. The measured acceleration response data and the AEKF approach are used to track the variation of the stiffness during the test. The tracking results for the stiffness variations correlate well with that of the referenced values. It is concluded that the AEKF approach is capable of tracking the variation of structural parameters leading to the detection of damages in nonlinear structures.

Key words: damage detection, adaptive extended Kalman filter, base-isolated structure

1. Introduction

High damping rubber-bearing isolation systems have been used in buildings and bridges. These base isolation systems will become more popular in the future due to their ability to reduce significantly the structural responses subject to earthquakes and other dynamic loads (Naeim and Kelly, 1999; Komodromos, 2000; Narasimhan *et al.*, 2006; Nagarajaiah *et al.*, 2008). To ensure the integrity and safety of these base isolation systems, a structural health monitoring system should be developed. In this regard, analysis techniques for damage identification of structures, based on vibration data measured from sensors, have received considerable attention. Various approaches to system identification and damage detection have been proposed in the literature, such as the least-square estimation (LSE) (Loh *et al.*, 2000; Lin *et al.*, 2001; Yang *et al.*, 2007), the extended Kalman filter (EKF) (Hoshiya and Saito, 1984; Sato *et al.*, 2001; Yang *et al.*, 2006; Zhou *et al.*, 2008; Yin *et al.*, 2012), unscented Kalman filter (UKF) (Wu and Smyth, 2008), sequential non-linear least-square estimation (SNLSE) (Huang and Yang, 2008), quadratic sum-squares error (QSSE) (Yang *et al.*, 2009), Monte Carlo filter (Sato and Chung, 2005), wavelet multiresolution technique (Chang and Shi, 2010), and others (e.g., Ching *et al.*, 2006; Yin and Zhou, 2006). In these techniques mentioned above, an adaptive tracking technique has been proposed for tracking the time-varying parameters on-line (e.g., Zhou *et al.*, 2008; Huang and Yang, 2008; Yang *et al.*, 2009). Simulation results demonstrate that this

adaptive EKF approach (AEKF) is capable of tracking the variations of structural parameters, such as the degradation of stiffness due to structural damages.

In this paper, experimental studies are performed and presented to verify the capability of the AEKF approach for identifying and tracking damages in nonlinear structures. Experimental tests using a base-isolated building model consisting of a scaled shear-beam type building model mounted on a rubber-bearing isolation system have been conducted in the laboratory. The Bouc-Wen model is selected to describe the non-linear behavior of rubber-bearings, which has the advantages of being smooth-varying. To simulate structural damages during the test, an innovative device, referred to as the stiffness element device (SED), is used herein to reduce the stiffness of the model. Different earthquake excitations have been used to drive the shake table, including the El Centro earthquake and Kobe earthquake. Various damage scenarios have been simulated and tested. Measured acceleration data and the AEKF approach are used to track the stiffness variation of the upper structure during the test. The experimental results demonstrate that the AEKF approach is capable of tracking the variation of structural parameters leading to the detection of damages in nonlinear structures.

2. Analytical model for Rubber-bearings

One challenging problem associated with the rubber-bearing isolator is the modeling of its nonlinear hysteretic behavior. Different hysteretic models for describing the dynamic behavior of rubber-bearings have been proposed in the literature, including the bi-linear model (Tan and Huang, 2000), tri-linear model (Furukawa *et al.*, 2005), Bouc-Wen model (Wen, 1989; Ma *et al.*, 2004; Yin *et al.*, 2010), etc. However, little test data are available aiming at the rigorous characterization of nonlinear hysteretic models (Abe *et al.*, 2004). Among these models, the Bouc-Wen model seems to be more flexible, involving more model parameters to be adjusted. Thus, the Bouc-Wen model is investigated to describe the hysteretic character of the rubber--bearings in this paper.

When subject to an earthquake acceleration $\ddot{x}_0(t)$, the equation of motion of rubber-bearing isolation system described by the uniaxial hysteretic Bouc-Wen model can be expressed as

$$m\ddot{x}(t) + R_T(x, z) = -m\ddot{x}_0(t) \tag{2.1}$$

where x is the relative displacement, z is a hysteretic variable, and m is the mass coefficient. The total restoring force $R_T(x, z)$ consists of elastic and hysteretic components as follows

$$R_T(x, z) = c\dot{x} + \alpha k x + (1 - \alpha)kz \tag{2.2}$$

where c and k are, respectively, the damping and stiffness coefficients, and $0 \leqslant \alpha \leqslant 1$ is the ratio of post-yielding stiffness to pre-yielding stiffness. The restoring force is purely hysteretic if $\alpha = 0$ and is purely elastic if $\alpha = 1$. The hysteretic variable is related to the relative displacement, and a general Bouc-Wen hysteresis model with degradation and pinching given by

$$\dot{z} = \frac{1}{\eta}h(z)[A\dot{x} - \nu(\beta|\dot{x}||z|^{n-1}z + \gamma\dot{x}|z|^n)] \tag{2.3}$$

In the above expression ν and η are degradation shape functions, and $h(z)$ is a pinching shape function. ν and η are defined as

$$\nu(\varepsilon) = 1 + \delta_1\varepsilon \qquad \eta(\varepsilon) = 1 + \delta_2\varepsilon \tag{2.4}$$

in which, δ_1 and δ_2 are two constant degradation parameters, ε is a quantity used as a measure of response duration and severity, introduced as follows

$$\varepsilon(t) = \int_0^t z\dot{x}\,dt \tag{2.5}$$

And the pinching function $h(z)$ takes the following form

$$h(z) = 1 - \zeta_1 \mathrm{e}^{-[z\,\mathrm{sgn}\,(\dot{x}) - qz_x]^2/\zeta_2^2} \tag{2.6}$$

where $\mathrm{sgn}\,(\dot{x})$ is the signum function of $\dot{x}$, and z_x is the ultimate value of z given by

$$z_x = \Big(\frac{A}{v(\beta + \gamma)}\Big)^{\frac{1}{n}} \tag{2.7}$$

The two functions $\zeta_1(\varepsilon)$ and $\zeta_2(\varepsilon)$ in Eq. (2.6) control the progress of pinching given by

$$\zeta_1(\varepsilon) = \zeta_s(1 - \mathrm{e}^{-p\varepsilon}) \qquad \zeta_2(\varepsilon) = (\psi + \delta_3\varepsilon)(\lambda + \zeta_1) \tag{2.8}$$

From Eqs. (2.2)-(2.8), there are 13 loop parameters (A, α, β, γ, n, δ_1, δ_2, ζ_s, q, p, ψ, δ_3 and λ) in the general Bouc-Wen model describing the hysteretic behavior. However, it has been shown that $A = 1$ is quite reasonable (Ma *et al.*, 2004), and hence it will be used in this study. Consequently, there remain 12 parameters (α, β, γ, n, δ_1, δ_2, ζ_s, q, p, ψ, δ_3 and λ) in the Bouc-Wen model. To ravel the contributions of these parameters to the system responses, the one-factor-at-a-time method (Ma *et al.*, 2004; Yin *et al.*, 2010) is adopted to address sensitivity of the 12 parameters relative to the chosen base values to understand the influence of each parameter on the system response.

As a typical example of local sensitivity analysis, a SDOF hysteretic structure subject to an earthquake acceleration $\ddot{x}_0(t)$ as shown in Eq. (2.1) is used. Selected base values are: $m = 125.53\,\mathrm{kg}$, $c = 0.07\,\mathrm{kNs/m}$, $k = 24.5\,\mathrm{kN/m}$, $\alpha = 0.2$, $\beta = 2$, $\gamma = 1$, $n = 2$, $\delta_1 = 0.02$, $\delta_2 = 0.02$, $\zeta_s = 0.8$, $q = 0.02$, $p = 1$, $\psi = 0.2$, $\delta_3 = 0.005$, and $\lambda = 0.1$. The scaled E-W component of the El Centro earthquake over a duration of 20 seconds is used as the excitation. Then, each of these 12 loop parameters is varied, one at a time, by up to $\pm 50\%$ from its base value while holding all other parameters at the base position. Denote the system response by $[x_1, x_2, x_3]^{\mathrm{T}} = [x, \dot{x}, R_T(x, z)]^{\mathrm{T}}$ at the base values and by $[y_1, y_2, y_3]^{\mathrm{T}}$ when one parameter, say w, is varied, where x, $\dot{x}$ and $R_T(x, z)$ denote the relative displacement, velocity and restoring force, respectively. A root-mean-square error is defined as follows

$$e_w = \sqrt{\frac{1}{M}\sum_{i=1}^{M}[(x_{1i} - y_{1i})^2 + (x_{2i} - y_{2i})^2 + (x_{3i} - y_{3i})^2]} \tag{2.9}$$

where $M = 1000$ is the number of sampling points with the sampling time of $\Delta t = 0.02\,\mathrm{s}$. As each w is varied over its range (from -50% to 50% of the base value), the maximum error

$$\|e_w\| = \max(e_w) \tag{2.10}$$

is recorded. These maximum values may be used as a measure of sensitivity. Based upon $\|e_w\|$, all the 12 loop parameters of the hysteretic model are ranked in Table 1 in the order of decreasing sensitivity for different earthquake intensities PGA (Peak ground acceleration). In order to consider the influence of the energy of the excitation, the results for three different PGAs of the excitations are also listed in Table 1. As can be observed from Table 1, although the order of the sensitivities of each parameter has slightly changed under different excitations, the parameters n, α, β and γ have remarkable influence on the response of the structure compared with the other eight parameters, i.e., δ_1, δ_2, ζ_s, q, p, ψ, δ_3 and λ. With several different sets of the base values, it is found that the sensitivity conclusion is the same as that obtained from sensitivity analysis above. Further, the above conclusion does not change when subject to another excitations, i.e., Kobe earthquake. It is emphasized that these conclusions are elicited based on the sets of base values and excitations used in this study.

Table 1. Parameter sensitivity ranking

Parameter	$\|e_w\|$					
w	PGA $= 0.3$ g	Rank	PGA $= 0.5$ g	Rank	PGA $= 1.0$ g	Rank
α	0.028	4	0.1281	4	0.7452	4
β	0.098	2	0.4716	2	2.8892	2
γ	0.04	3	0.1914	3	1.2095	3
n	5.137	1	11.6161	1	28.7566	1
δ_1	0	11	0	11	0.0005	11
δ_2	0.001	10	0.0027	10	0.0317	9
ζ_s	0.008	7	0.0234	7	0.2156	5
q	0.005	9	0.0103	9	0.029	10
p	0.008	7	0.0234	7	0.2149	6
ψ	0.0083	5	0.0293	5	0.2099	7
δ_3	0	11	0	11	0	12
λ	0.0083	5	0.0291	6	0.202	8

From the results of the parameter sensitivity analysis above, it seems that the contributions of these degradation and pinching parameters could gnored. In order to determine the final hysteretic model for the rubber-bearings, i.e., the parameters contained in the Bouc-Wen model, a performance testing on the GZN110 rubber-bearing is conducted as shown in Fig. 1a. Sinusoidal excitations with different frequencies are used to drive the actuator, and the displacement-force curves of the rubber bearing under different excitation frequencies are given in Fig. 1b. It is observed from Fig. 1b that there are no significant effects of degradation and pinching. For this reason, we consider the hysteretic model for the rubber-bearings without degradation and pinching, i.e., $\delta_1 = 0$, $\delta_2 = 0$ and $\zeta_s = 0$ for simplicity. Then, the unknown hysteresis loop parameters in the Bouc-Wen model are reduced to α, β, γ and n. Equation (2.3) could be rewritten as

$$\dot{z} = \dot{x} - \beta |\dot{x}|\, |z|^{n-1} z - \gamma \dot{x} |z|^n \tag{2.11}$$
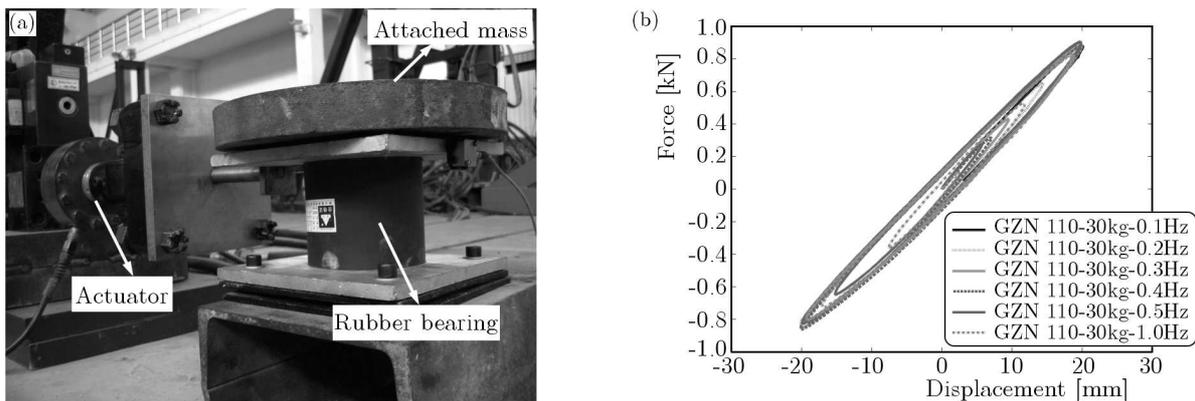
Fig. 1. (a) Performance testing on GZN 110 rubber bearing; (b) force-displacement curves of GZN 110 rubber bearing

Kasalanati and Constantinou (1999) have proposed that $A/(\beta + \gamma) = 1$. Chen *et al.* (2006) used $A = 1$, $\beta = 0.1$, $\gamma = 0.9$, $n = 2$ for the laminated and stirruped rubber bearings. Huang and Zhao (2000) used $A = 1$, $\beta = 0.5$, $\gamma = 0.5$, $n = 3$ for the laminated rubber bearings. Yin *et al.* (2010, 2012) also suggested that $A = 1$, $\beta = 0.5$, $\gamma = 0.5$, $n = 2$ for rubber bearings. In this

paper, these parameter values suggested by Yin *et al.* (2010, 2012) are adopted for a reference, and the following experimental results are compared with these suggested values.

3. Adaptive extended Kalman filter

In this section, a brief summary of the adaptive extended Kalman filter (AEKF) approach to be used is given, and the details are referred to Yang *et al.* (2006). Consider a m-DOF structure with the displacement vector $\mathbf{x}$, and velocity vector $\dot{\mathbf{x}}$. Let us introduce an extended state vector, $\mathbf{Z}(t) = \{\mathbf{x}^\mathrm{T}, \dot{\mathbf{x}}^\mathrm{T}, \boldsymbol{\theta}^\mathrm{T}\}^\mathrm{T}$, where $\boldsymbol{\theta}^\mathrm{T} = [\theta_1, \theta_2, \dots, \theta_n]^\mathrm{T}$ is an n-unknown parametric vector with θ_i $(i = 1, 2, \dots, n)$ being the i-th unknown parameter of the structure, including damping, stiffness, nonlinear and hysteretic parameters. In what follows, the boldface letter represents either a vector or a matrix. The vector equation of motion of the structure can be expressed as

$$\frac{d\mathbf{Z}(t)}{dt} = \mathbf{g}(\mathbf{Z}, \mathbf{f}, t) + \mathbf{w}(t) \tag{3.1}$$

in which $\mathbf{w}(t)$ is the model noise (uncertainty) vector with zero mean and a covariance matrix $\mathbf{Q}(t)$, and $\mathbf{f}$ is the excitation vector. A nonlinear discrete vector equation for an observation vector (measured responses) can be expressed as follows

$$\mathbf{Y}_{k+1} = \mathbf{h}(\mathbf{Z}_{k+1}, \mathbf{f}_{k+1}, k+1) + \mathbf{v}_{k+1} \tag{3.2}$$

in which $\mathbf{Y}_{k+1}$ is a l-dimensional observation (measured) vector at $t = (k+1)\Delta t$ (sampling time step Δt), i.e., $\mathbf{Y}_{k+1} = \mathbf{Y}(t = (k+1)\Delta t)$, $\mathbf{Z}_{k+1} = \mathbf{Z}(t = (k+1)\Delta t)$, and $\mathbf{f}_{k+1} = \mathbf{f}(t = (k+1)\Delta t)$. In Eq. (3.2), $\mathbf{v}_{k+1}$ is a measurement noise vector assumed to be a Gaussian white noise vector with zero mean and a covariance matrix $E[\mathbf{v}_k \mathbf{v}_j^\mathrm{T}] = \mathbf{R}_k \delta_{kj}$, where δ_{kj} is the Kronecker delta.

Let $\widehat{\mathbf{Z}}_{k+1|k+1}$ be the estimate of $\mathbf{Z}_{k+1}$ at $t = (k+1)\Delta t$, and $\widehat{\mathbf{Z}}_{k+1|k}$ be the estimate of $\mathbf{Z}_{k+1}$ at $t = k\Delta t$. The recursive solution for the estimate $\widehat{\mathbf{Z}}_{k+1|k+1}$ of the extended state vector is given by

$$\begin{aligned}
\widehat{\mathbf{Z}}_{k+1|k+1} &= \widehat{\mathbf{Z}}_{k+1|k} + \mathbf{K}_{k+1}[\mathbf{Y}_{k+1} - \mathbf{h}(\widehat{\mathbf{Z}}_{k+1|k}, \mathbf{f}_{k+1}, k+1)] \\
\widehat{\mathbf{Z}}_{k+1|k} &= E\{\mathbf{Z}_{k+1}|\mathbf{Y}_1, \mathbf{Y}_2, \dots, \mathbf{Y}_k\} = \widehat{\mathbf{Z}}_{k|k} + \int_{k\Delta t}^{(k+1)\Delta t} \mathbf{g}(\widehat{\mathbf{Z}}_{t|k}, \mathbf{f}, t) \, dt
\end{aligned} \tag{3.3}$$

in which $\mathbf{K}_{k+1}$ is the Kalman gain matrix

$$\mathbf{K}_{k+1} = P_{k+1|k}\mathbf{H}_{k+1|k}^\mathrm{T}[\mathbf{H}_{k+1|k}\mathbf{P}_{k+1|k}\mathbf{H}_{k+1|k}^\mathrm{T} + \mathbf{R}_{k+1}]^{-1} \tag{3.4}$$

In Eq. (3.4), $\mathbf{P}_{k+1|k}$ and $\mathbf{H}_{k+1|k}$ are given by

$$\begin{aligned}
P_{k+1|k} &= \boldsymbol{\Lambda}_{k+1}[\boldsymbol{\Phi}_{k+1,k}\mathbf{P}_{k|k}\boldsymbol{\Phi}_{k+1,k}^\mathrm{T}]\boldsymbol{\Lambda}_{k+1}^\mathrm{T} + \mathbf{Q}_{k+1} \\
\mathbf{H}_{k+1|k} &= \left[\frac{\partial \mathbf{h}(\mathbf{Z}_{k+1}, \mathbf{f}_{k+1}, k+1)}{\partial \mathbf{Z}_{k+1}}\right]_{\mathbf{Z}_{k+1} = \widehat{\mathbf{Z}}_{k+1|k}}
\end{aligned} \tag{3.5}$$

where $\boldsymbol{\Phi}_{k+1,k}$ is the transition matrix of the extended state vector from $\mathbf{Z}_k$ to $\mathbf{Z}_{k+1}$, and $\mathbf{P}_{k|k}$ is given by

$$\mathbf{P}_{k|k} = [\mathbf{I}_{2m+n} - \mathbf{K}_k\mathbf{H}_{k|k-1}]\mathbf{P}_{k|k-1}[\mathbf{I}_{2m+n} - \mathbf{K}_k\mathbf{H}_{k|k-1}]^\mathrm{T} + \mathbf{K}_k\mathbf{R}_k\mathbf{K}_k^\mathrm{T} \tag{3.6}$$

In Eq. (3.5)$_1$, $\boldsymbol{\Lambda}_{k+1}$ is a diagonal matrix referred to as the adaptive factor matrix. The determination of $\boldsymbol{\Lambda}_{k+1}$ has been described in Yang *et al.* (2006). In the recursive solution above,

$\mathbf{P}_{k|k}$ is the error covariance matrix of the estimated extended state vector. To initiate the recursive solution, the initial values for the unknown extended state vector $\mathbf{Z}(t) = \{\mathbf{x}^{\mathrm{T}}, \dot{\mathbf{x}}^{\mathrm{T}}, \boldsymbol{\theta}^{\mathrm{T}}\}^{\mathrm{T}}$, including the unknown parameters and the unknown state vector, should be estimated. Likewise, the initial error covariance matrix $\mathbf{P}_{0|0}$ of the estimated extended state vector, the covariance matrix $\mathbf{R}$ of the measurement noise vector $\mathbf{v}(t)$, and the covariance matrix $\mathbf{Q}$ of the system noise vector $\mathbf{w}(t)$ should be assigned as will be described later. Finally, in computing the adaptive factor matrix $\boldsymbol{\Lambda}_{k+1}$ for the on-line damage identification, a constrained optimization procedure was used, in which a small number (constraint) $\delta = 0.01$ was suggested. Further, in computing the covariance matrix of the predicted output error, it was suggested by Yang *et al.* (2006) that $\mathbf{G}_{1,0} = \mathbf{0}$, $G_{2,0} = 0$. These values, i.e., $\delta = 0.01$, $\mathbf{G}_{1,0} = \mathbf{0}$ and $G_{2,0} = 0$, will be used in the following analysis of all experimental data.

4. Experimental studies

4.1. Experimental set-up

Rubber-bearings GZN110 supplied by Hengshui Zhentai Seismic Isolation Instrument CO., LTD were used as the base isolator. The base-isolation system consists of 8 circular rubber-bearings each with a diameter of 11 cm and an upper floor mate. A 400 mm by 300 mm small-scale shear-beam type building model mounted on a 600 mm by 500 mm floor mate of the rubber-bearing isolation system, as shown in Figs. 2a is used for the experiments. The base-isolated building can be simplified to be a 2-DOF shear-beam model consisting of an upper storey and an isolation storey, as shown in Fig. 2b. The total height of this building model is 660 mm, where the height of upper storey is 345 mm and the height of the isolation storey is 315 mm. The total weight of the model is 350 kg, in which the mass of the upper floor is 50 kg and the mass of the base mate is 300 kg. The first two natural frequencies of the test specimen are: 1.955 Hz and 5.376 Hz, respectively. Based on the discretized 2-DOF shear-beam model, the stiffness of each story was estimated to be 52 kN/m and 46 kN/m, respectively, using the finite-element approach. The base-isolated building model was placed on the shake table that simulates different kinds of earthquakes. Two earthquake excitations were used, including the El Centro and the Kobe earthquakes. During the tests, each floor was installed with one acceleration sensor and one displacement sensor to measure the floor responses.
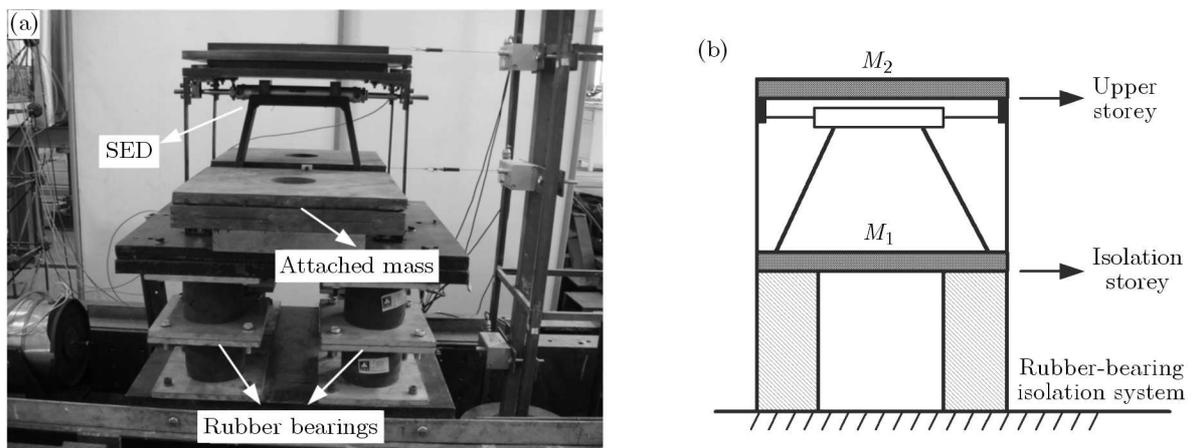
Fig. 2. (a) The based-isolated building model on the shake table; (b) schematic figure for the rubber-bearing isolated building (shear-beam model)

The damage in a storey unit is assumed to be reflected by the reduction of its stiffness. To simulate the reduction of stiffness in the upper storey, a stiffness element device (SED),

consisting of a hydraulic cylinder-piston (HCP) and a bracing system, with an effective stiffness of K_{hi} is installed in the upper storey, so that stiffness of the upper storey is increased by K_{hi}. During the experimental test, the effective stiffness of the SED is reduced to zero to simulate the reduction of the stiffness in the upper storey.

During the tests, the shake table and the masses were each installed with one acceleration sensor and one displacement sensor to measure the responses. The absolute acceleration responses of the isolation storey a_1, and the upper storey a_2, as well as the earthquake ground acceleration a_d were measured. Also, the displacements of each storey and the base were measured for the correlation study.

4.2. Experimental results

To demonstrate the capability and accuracy of the adaptive extended Kalman filter (AEKF) approach for tracking the damage of base-isolated structures, experimental tests were conducted herein for different damage scenarios. For shake table tests, two earthquakes will be used, including the El Centro earthquake scaled to a peak ground acceleration (PGA) of 0.6 g and the Kobe earthquake scaled to a PGA of 0.5 g. For each earthquake, the acceleration responses (a_1, a_2) of both floors and the shake table acceleration a_d were measured. The sampling frequency of all measurements was 500 Hz. To identify the parameters of the rubber-bearing isolated structure, and to track the damage in the upper storey when it occurs, different unknown parameters in the Bouc-Wen model will be considered. From the hysteresis loop shown in Fig. 1b, the effects of degradation and pinching are negligible. Further, from the sensitivity analysis conducted in the previous section, only four loop parameters, i.e., α, β, γ, n in Bouc-Wen model for the isolation system will be considered in this study.

4.2.1. Bouc-Wen model I (3 unknown parameters for isolation system)

First, we consider the loop parameters β, γ and n of the Bouc-Wen model for the isolation storey to be constants, i.e., $\beta = 0.5$, $\gamma = 0.5$ and $n = 2$. Hence, the unknown parameters for the isolation system consist of c, k and α. Hence, the hysteretic non-linear equation can be rewritten as

$$\dot{z} = \dot{x} - \frac{1}{2}|\dot{x}|\,|z|z - \frac{1}{2}\dot{x}|z|^2 \qquad (4.1)$$

Case 1: El Cento earthquake (PGA = 0.6 g)

In this test, a stiffness element device (SED) is installed in the upper storey unit as shown in Fig. 2. The cylinder of the SED is filled by air with an air pressure of 0.7 MPa. From the experimental test, the air pressure at $P_0 = 0.7$ MPa results in an effective stiffness of 7.0 kN/m for the SED, i.e., $K_{hi} = 7.0$ kN/m. Thus, the stiffness of the upper storey was estimated to be $k_2 = 53$ kN/m, whereas the stiffness of the base-isolated storey was estimated to be $k_1 = 52$ kN/m. During the test with the El Centro earthquake excitation, both valves of the SED unit were open simultaneously at $t = 14$ seconds, so that the stiffness of the upper storey reduces abruptly from 53 kN/m to 46 kN/m at $t = 14$ seconds. The acceleration responses of both floors and the shake table acceleration, a_1, a_2 and a_d in m/s^2, were measured and presented in Fig. 3. Further, the displacement responses of both floors and the base were also measured for correlation studies later.

For the AEKF approach, the test specimen is considered as a 2-DOF shear-beam building model, and the equations of motion can be written, in which the stiffness and damping of each storey as well as the nonlinear hysteretic parameters of the base-isolator, are unknown parameters. Consequently, the vector equation of motion, Eq. (3.1), for the extended state vector
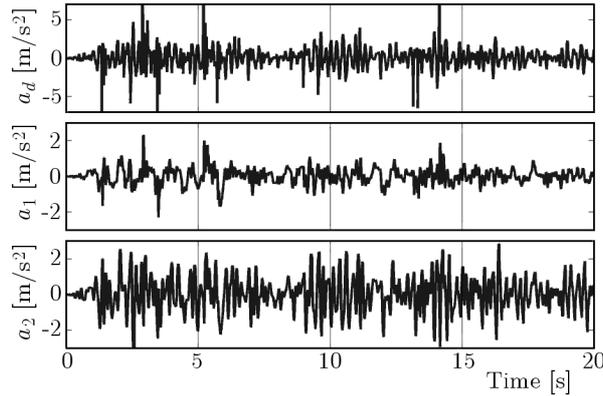
Fig. 3. Measured acceleration responses and shake table acceleration due to El Centro earthquake

can be established analytically. With the measured shake table acceleration ad and acceleration responses (a_1, a_2) shown in Fig. 3, the unknown structural parameters, i.e., k_i, c_i $(i = 1, 2)$, and α can be identified on-line using the recursive solution, Eqs. (3.3)-(3.6), of the AEKF approach.

For the AEKF recursive solution described previously, the following initial values are assumed: (i) the initial values for k_i and c_i are: $k_{i0} = 40\,\text{kN/m}$ and $c_{i0} = 0.1\,\text{kNs/m}$ $(i = 1, 2)$, (ii) the initial values for the displacements and velocities are zero, i.e., $\mathbf{x} = [0, 0]^\text{T}$, $\dot{\mathbf{x}} = [0, 0]^\text{T}$, (iii) the initial error covariance matrix $\mathbf{P}_{0|0}$ of the extended state vector is a (10×10) diagonal matrix with the first 5 diagonal elements being 1 and the last 5 diagonal elements being 1000, and (iv) the covariance matrices of the measurement noise vector $\mathbf{v}(t)$ and the system noise vector $\mathbf{w}(t)$ are chosen to be $\mathbf{R} = 0.1\mathbf{I}_2$ and $\mathbf{Q} = 10^{-9}\mathbf{I}_{10}$, respectively, where $\mathbf{I}_j$ is a $(j \times j)$ unit matrix. In the following experimental studies in Case 1 and Case 2 to be presented later, these same initial values will be used.
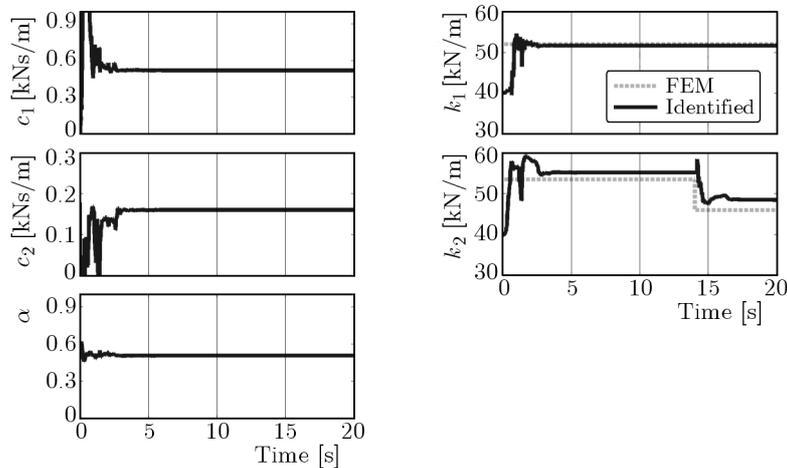
Fig. 4. The identified system parameters, Case 1: El Centro earthquake

Based on the AEKF recursive solution and the measured data, the identified unknown parameters for both storeys are presented in Fig. 4 as solid curves (black color). Also shown in Fig. 4 as dashed curves (grey color) for comparison are the estimated results based on the finite-element method. Further, the identified inter-storey drifts (x_1, x_2) and displacements (d_1, d_2) of each floor using the AEKF approach are presented in Fig. 5 as solid curves (black color), whereas the dashed curves (grey color) are the measured experimental results for comparison. The identified numerical results based on the AEKF approach are as follows: (i) prior to damage, $k_1 = 51.7\,\text{kN/m}$ and $k_2 = 55.2\,\text{kN/m}$, and (ii) after damage, $k_1 = 51.7\,\text{kN/m}$ and

$k_2 = 48.5 \, \text{kN/m}$. It is observed from both Fig. 4 (solid curves) and the numerical results above that the identified structural parameters based on the AEKF approach are very reasonable in comparison with that estimated by the finite element method (dashed curves). The difference between the solid and dashed curves has been expected due to the structural uncertainty of the test model, including the shear-beam assumption. Figures 4 and 5 clearly demonstrate that the AEKF approach is capable of tracking the variation of stiffness parameters, leading to the detection of structural damages.
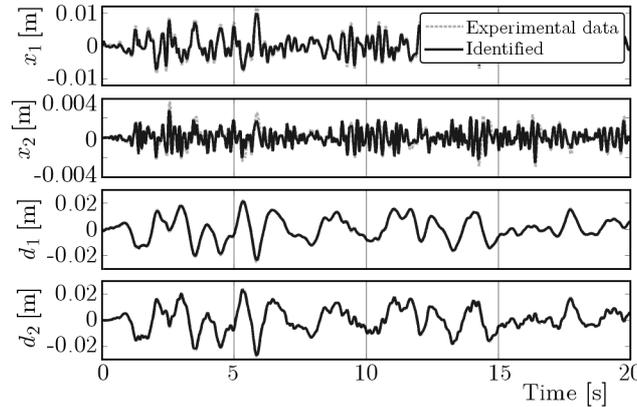
Fig. 5. The identified relative and absolute displacements, Case 1: El Centro earthquake

Case 2: Kobe earthquake (PGA = 0.5 g)

Instead of the El Centro earthquake, the Kobe earthquake was used to drive the shake table. The test configuration is identical to that of Case 1 presented previously, except that the air pressure of the SED installed in the first storey is $P_0 = 0.75 \, \text{MPa}$. This results in a stiffness of $7.5 \, \text{kN/m}$ for the SED. Hence, the stiffness of the upper storey prior to damage is $k_2 = 46 \, \text{kN/m} + 7.5 \, \text{kN/m} = 53.5 \, \text{kN/m}$, whereas the stiffness of the base isolator remains the same, i.e., $k_1 = 52 \, \text{kN/m}$. During the test, valves of the SED were open at $t = 8.0$ seconds following the most intensive portion of the earthquake. After $t = 8.0$ seconds, k_2 is reduced to $46 \, \text{kN/m}$. Acceleration responses (a_1, a_2) of both floors and the shake table acceleration a_d were measured and presented in Fig. 6. Based on the measured data in Fig. 6 and the AEKF approach, the identified unknown parameters for both storeys are presented in Fig. 7 as solid curves (black color), whereas the dashed curves (grey color) are the finite-element results. The predicted inter-storey drifts (x_1, x_2) and displacements (d_1, d_2) of each floor are presented in Fig. 8 as solid curves (black color), whereas the dashed curves (grey color) are the measured data for comparison. The identified numerical results using the AEKF approach are as follows: (i) prior to damage, $k_1 = 52.2 \, \text{kN/m}$ and $k_2 = 55.6 \, \text{kN/m}$, and (ii) after damage, $k_1 = 52.2 \, \text{kN/m}$ and $k_2 = 47.6 \, \text{kN/m}$. As observed from Figs. 7 and 8, the AEKF predictions are quite reasonable, and that the trend of predictions is consistent with that of the previous case.

4.2.2. Bouc-Wen Model II (5 unknown parameters for isolation system)

In this situation, we consider the parameter n of the Bouc-Wen model for the isolation storey to be 2.0, i.e., $n = 2$, and the other loop parameters, α, β, and γ to be unknown in Eqs. (2.2) and (2.11). Then, the hysteretic non-linear equation can be rewritten as

$$\dot{z} = \dot{x} - \beta |\dot{x}| \, |z| z - \gamma \dot{x} |z|^2 \tag{4.2}$$

For the AEKF recursive solution, the initial values assumed for Case 3 and Case 4 are similar to that of Case 1 and 2, except that $\mathbf{P}_{0|0}$ is a (12×12) diagonal matrix with the first 5 diagonal
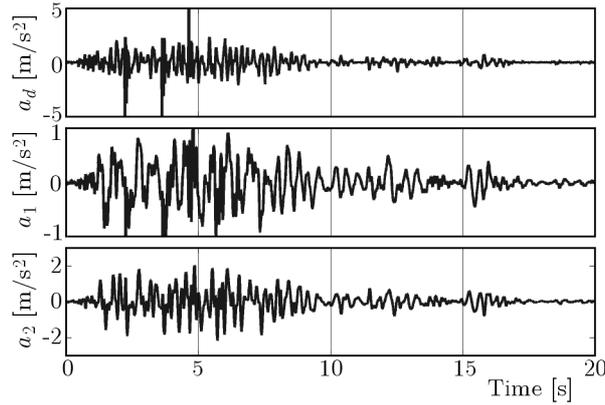
Fig. 6. Measured acceleration responses and shake table acceleration due to Kobe earthquake
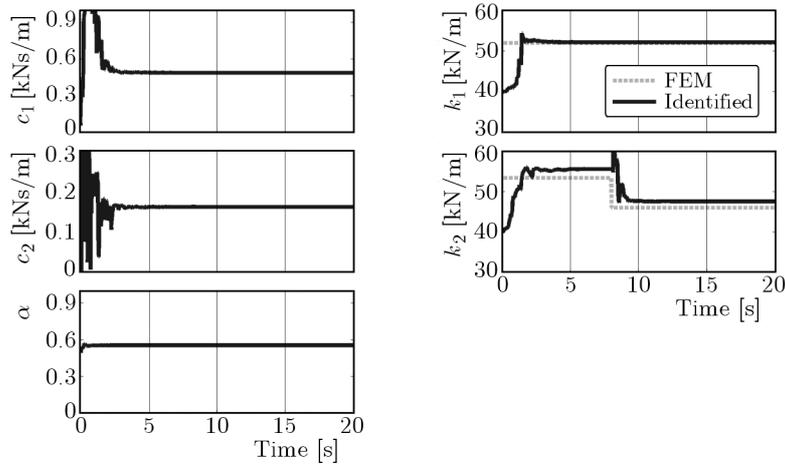
Fig. 7. The identified model parameters, Case 2: Kobe earthquake
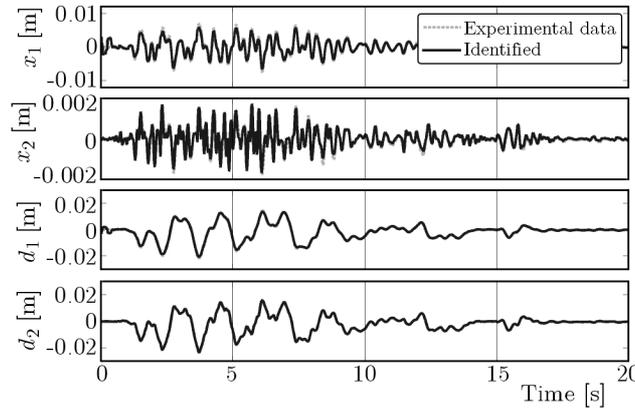
Fig. 8. The identified relative and absolute displacements, Case 2: Kobe earthquake

elements being 1 and the last 7 diagonal elements being 1000, $\mathbf{R} = 0.1\mathbf{I}_2$ and $\mathbf{Q} = 10^{-9}\mathbf{I}_{10}$. In the following experimental studies in Case 3 and Case 4 to be presented, these initial values will be used. Note that these initial values are basically identical to that of Case 1 and Case 2.

Case 3: El Centro earthquake (PGA = 0.6 g)

Similar to Case 1, a scaled El Centro earthquake was applied to the base. Based on the acceleration measurements shown in Fig. 3 and the AEKF solution, the identified parameters

are presented in Fig. 9. Further, the identified displacements are shown in Fig. 10 as black solid curves, whereas the measured displacements are shown as grey dashed curves for comparison. It is observed from Fig. 10 that the identified displacements match the experimental ones well.
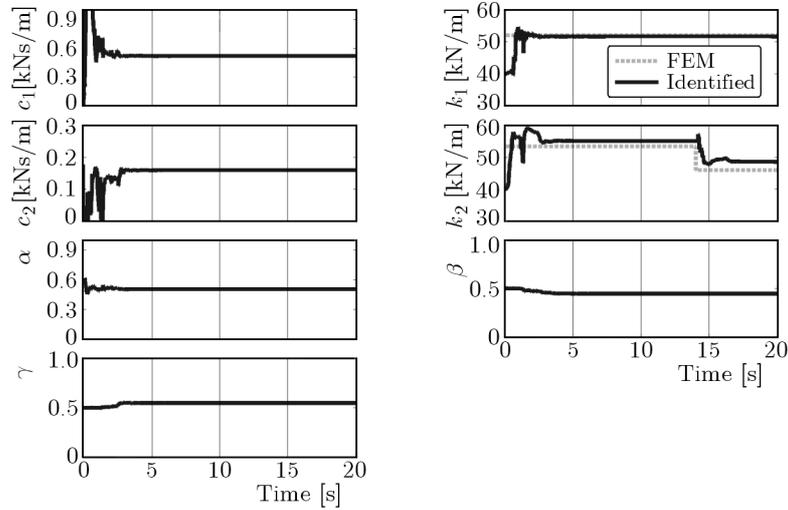
Fig. 9. The identified model parameters, Case 3: El Centro earthquake
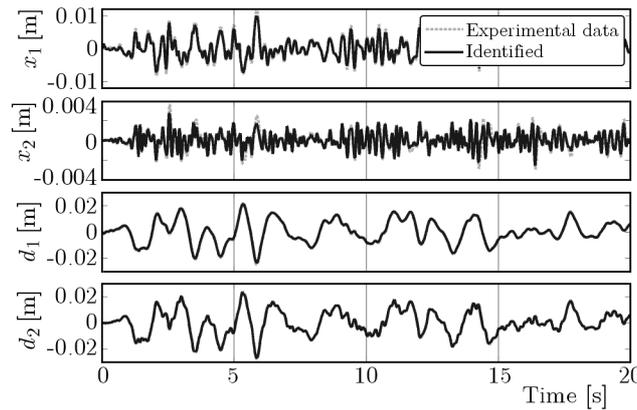
Fig. 10. The identified relative and absolute displacements, Case 3: El Centro earthquake

Case 4: Kobe earthquake (PGA $= 0.5$ g)

Similar to Case 2, a scaled Kobe earthquake was applied to the base. Based on the acceleration measurements shown in Fig. 6 and the AEKF solution, the identified parameters are presented in Fig. 11. As observed from Fig. 11, all parameters converge nicely after 2.5 seconds. The identified displacements are shown in Fig. 12 as black solid curves, whereas the measured displacements are shown as grey dashed curves for comparison. Again, the AEKF approach is capable of identifying structural damages.

5. Conclusions

Recently, a new adaptive extended Kalman filter (AEKF) has been proposed for the on-line damage identification of structures based on simulation results. In this paper, we have performed experimental studies to verify the capability of this AEKF in identifying the damage of
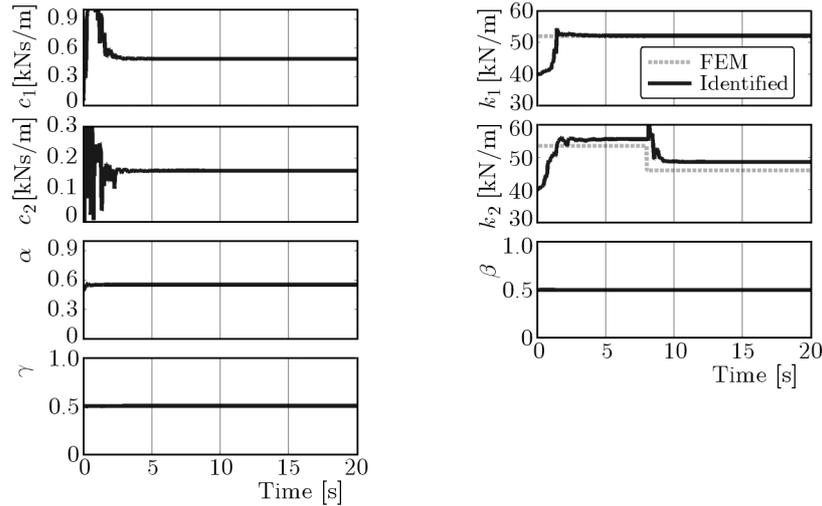
Fig. 11. The identified model parameters, Case4: Kobe earthquake
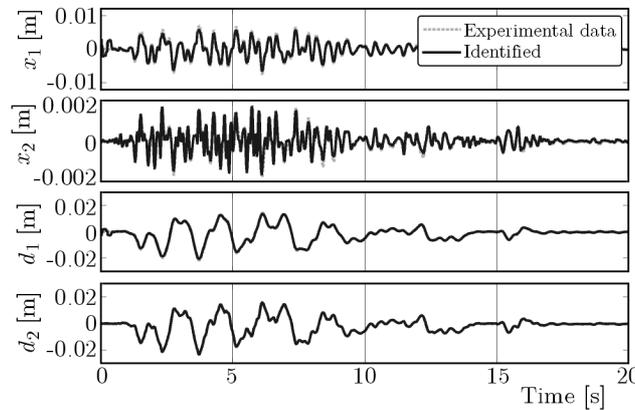
Fig. 12. The identified relative and absolute displacements, Case 4: Kobe earthquake

base-isolated structures by conducting a series of experimental tests on a scaled rubber-bearing isolated building model. The Bouc-Wen models with 3 and 5 unknown parameters, respectively, have been investigated to represent the hysteretic behavior of rubber-bearing isolators. To simulate the structural damage during the test, an innovative stiffness element device (SED) has been used to reduce the stiffness of the upper storey. Different damage scenarios under different earthquakes have been simulated and tested. The measured acceleration response data and the AEKF approach have been used to identify the unknown structural parameters, and to track the stiffness variation of the structure during the test. The identified stiffness parameters based on the AEKF approach correlate reasonably well with those estimated by the finite-element method despite the stiffness of the upper storey is uniformly bigger than that estimated by the finite-element method. This trend is consistent for all the test results, including different loading conditions and different damage scenarios. Such discrepancies have been expected due to the structural uncertainties of the test model. Experimental studies conducted herein demonstrate that the AEKF approach is capable of: (i) identifying nonlinear structural parameters, and (ii) tracking the variation of stiffness parameters leading to the detection of structural damages. In addition to the AEKF approach, the initial values, such as the initial parametric values and the covariance matrices of the measurement noise vector $\mathbf{v}(t)$, have an important influence on the stability and convergence of the AEKF and, consequently, on the estimations of the structural parameter and the measured noise level, e.g., stiffness coefficients k_i and $\mathbf{R}$, conducted previously and experientially.

References

1. ABE M., YOSHIDA J., FUJINO Y., 2004, Multi-axial behaviors of laminated rubber bearings and their modeling I: Experimental study, *Journal of Structural Engineering, ASCE*, **130**, 8, 1119-1132

2. BABER T.T., WEN Y.K., 1981, Random vibration of hysteretic degrading system, *Journal Engineering Mechanics, ASCE*, **107**, 1069-1087

3. CHANG C.C., SHI Y.F., 2010, Identification of time-varying hysteretic structures using wavelet multiresolution analysis, *International Journal of Nonlinear Mechanics*, **45**, 1, 21-34

4. CHEN B.J., TSAI C.S., CHUNG L.L., CHIANG T.C., 2006, Seismic behavior of structures isolation with a hybrid system of rubber bearings, *Structural Engineering Mechanics*, **22**, 6, 761-783

5. CHING J., BECK J.L., PORTER K.A., SHAIKHUTDINOV R., 2006, Bayesian state estimation method for nonlinear systems and its application to recorded seismic response, *Journal of Engineering Mechanics*, **132**, 4, 396-410

6. FURUKAWA T., ITO M., NOORI M.N., 2005, System identification of base-isolated building using seismic response data, *Journal of Engineering Mechanics, ASCE*, **131**, 3, 268-273

7. HOSHIYA M., SAITO E., 1984, Structural identification by extended Kalman filter, *Journal of Engineering Mechanics, ASCE*, **110**, 12, 1757-1771

8. HUANG H., YANG J.N., 2008, Damage identification of substructure for local health monitoring, *Smart Structures and Systems*, **4**, 6, 795-807

9. HUANG J.W., ZHAO B., 2000, The nonlinear dynamic response of multistory base isolated building with laminated rubber bearings, *Journal of Xi'an University of Science and Technology*, **20**, 4, 317-321

10. KASALANATI A., CONSTANTINOU M.C., 1999, Experimental study of bridge elastomeric and other isolation and energy dissipation system with emphasis on uplift prevention and high velocity near-source seismic excitation, Technical Report MCEER-99-0004, University at Buffalo, State University of New York, U.S.A.

11. KOMODROMOS P., 2000, *Seismic Isolation for Earthquake-Resistant Structures*, WIT Press, Ashurst Lodge, Sons, Inc.

12. LIN J.W., BETTI R., SMYTH A.W., LONGMAN R.W., 2001, On-line identification of nonlinear hysteretic structural system using a variable trace approach, *Earthquake Engineering and Structural Dynamics*, **30**, 9, 1279-1303

13. LOH C.H., LIN C.Y., HUANG C.C., 2000, Time domain identification of frames under earthquake loadings, *Journal of Engineering Mechanics, ASCE*, **126**, 7, 693-703

14. MA F., ZHANG H., BOCKSTEDTE A, FOLIENTE G.C., PAEVERE P., 2004, Parameter analysis of the differential model of hysteresis, *Journal of Applied Mechanical, ASME*, **71**, 3, 342-349

15. NAEIM F., KELLY J.M., 1999, *Design of Seismic Isolated Structures – From Theory to Practice*, John Wiley & Sons, Inc.

16. NARASIMHAN S., NAGARAJAIAH S., JOHNSON E.A., GAVIN H.P., 2006, Smart base-isolated benchmark building. Part I: Problem definition, *Structural Control and Health Monitoring*, **13**, 2/3, 573-588

17. NAGARAJAIAH S., NARASIMHAN S., JOHNSON E., 2008, Structural control benchmark problem: Phase II – Nonlinear smart base-isolated building subjected to near-fault earthquakes, *Structural Control and Health Monitoring*, **15**, 5, 653-656

18. SATO T., CHUNG M., 2005, Structural identification using adaptive Monte Carlo filter, *Journal of Structural Engineering, JSCE*, **51**, 471-477

19. SATO T., HONDA R., SAKANOUE T., 2001, Application of adaptive Kalman filter to identify a five story frame structure using NCREE experimental data, *Proceedings of Structural Safety and Reliability, ICOSSA2001*, Swets & Zeitinger: Lisse, 2001, CD-ROM, 7 pages

20. TAN R.Y., HUANG M.C., 2000, System identification of a bridge with lead-rubber bearings, *Computers and Structures*, **74**, 267-280

21. WEN Y.K., 1989, Methods of random vibration for inelastic structures, *Applied Mechanical Reviews*, **42**, 2, 39-52

22. WU M.L., SMYTH A., 2008, Real-time parameter estimation for degrading and pinching hysteretic models, *International Journal of Nonlinear Mechanics*, **43**, 9, 822-833

23. YANG J.N., HUANG H.W., PAN S.W., 2009, Adaptive quadratic sum-squares error for structural damage identification, *Journal of Engineering Mechanics, ASCE*, **135**, 2, 67-77

24. YANG J.N., LIN S., HUANG H., ZHOU L., 2006, An adaptive extended Kalman filter for structural damage identification, *Structural Control and Health Monitoring*, **13**, 4, 849-867

25. YANG J.N., PAN S., LIN S., 2007, Least square estimation with unknown excitations for damage identification of structures, *Journal of Engineering Mechanics, ASCE*, **133**, 1, 12-21

26. YIN Q., ZHOU L., 2006, Non-linear structural identification using a recursive model reference adaptive Algorithm, *Journal of Vibration Engineering*, **19**, 3, 341-345

27. YIN Q., ZHOU L., MU T.F., YANG J.N., 2012, System identification of rubber-bearings based on experimental tests, *Journal of Vibroengineering*, **14**, 1, 315-324

28. YIN Q., ZHOU L., WANG X.M., 2010, Parameter identification of hysteretic model of rubber-bearing based on sequential nonlinear least-square estimation, *Earthquake Engineering and Engineering Vibration*, **9**, 3, 375-383

29. ZHOU L., WU S.Y., YANG J.N., 2008, Experimental study of an adaptive extended Kalman filter for structural damage identification, *Journal of Infrastructure Systems, ASCE*, **14**, 1, 42-51